

On the magnetic structure and wind parameter profiles of Alfvén wave driven winds in late-type supergiant stars

D. Falceta-Gonçalves^{1*}, A. A. Vidotto¹ and V. Jatenco-Pereira¹

¹*Instituto de Astronomia, Geofísica e Ciências Atmosféricas,*

Universidade de São Paulo, Rua do Matão 1226, CEP 05508-900, São Paulo, Brazil

ABSTRACT

Cool stars at giant and supergiant evolutionary phases present low velocity and high density winds, responsible for the observed high mass-loss rates. Although presenting high luminosities, radiation pressure on dust particles is not sufficient to explain the wind acceleration process. Among the possible solutions to this still unsolved problem, Alfvén waves are, probably, the most interesting for their high efficiency in transferring energy and momentum to the wind. Typically, models of Alfvén wave driven winds result in high velocity winds if they are not highly damped. In this work we determine self-consistently the magnetic field geometry and solve the momentum, energy and mass conservation equations, to demonstrate that even a low damped Alfvén wave flux is able to reproduce the low velocity wind. We show that the magnetic fluxtubes expand with a super-radial factor $S > 30$ near the stellar surface, larger than that used in previous semi-empirical models. The rapid expansion results in a strong spatial dilution of the wave flux. We obtained the wind parameter profiles for a typical supergiant star of $16 M_{\odot}$. The wind is accelerated in a narrow region, coincident with the region of high divergence of the magnetic field lines, up to 100 km s^{-1} . For the temperature, we obtained a slight decrease near the surface for low damped waves, because the wave heating mechanism is less effective than the radiative losses. The peak temperature occurs at $r \simeq 1.5 r_0$ reaching 6000 K . Propagating outwards, the wind cools down mainly due to adiabatic expansion.

Key words: stars: mass loss; stars: magnetic fields; MHD; waves

1 INTRODUCTION

Cool giant and supergiant stars are known to present continuous mass loss process occurring at high rates, typically $10^{-10} - 10^{-5} M_{\odot} \text{ yr}^{-1}$, but in low velocity winds ($u_{\infty} < 300 \text{ km s}^{-1}$) (Dupree 1986, Lamers & Cassinelli 1999). After decades of theoretical and observational studies, the mechanisms in which the wind acceleration occurs are still poorly understood. Due to the stellar high luminosity and low effective temperature several authors have proposed radiatively dust driven models to explain the observed wind properties (Liberatore, Lafon & Berruyer 2001, Elitzur & Ivezic 2001, Woitke & Niccolini 2005). At the pulsating phase, acoustic waves generate high density shells that could allow dust to form near the stellar surface. In this scenario, radiative pressure on grains transfers momentum to these particles being responsible for their acceleration and, if gas and dust are dynamically well coupled, grains drag the gas outwards resulting in the mass ejection. However, at stationary envelopes (*e.g.* pre-AGB phase) dust driven theoretical

models have lately failed in reproducing the wind properties, mainly because the dust-gas coupling is not effective (Sandín & Hofner 2003). Observationally, Guandalini *et al.* (2005) found no strong correlation between the mass loss rates and the luminosities of AGB stars. Their main conclusion is that, if radiative pressure is important in powering these stellar winds, it must occur in addition to other mechanism. Another drawback to the radiation pressure models is the need for the dust formation region to be close to the star. Recent high resolution Doppler measurements show that winds are mainly accelerated near the stellar surface ($r < 1.3 R_{*}$) (Airapetian, Carpenter & Ofman 2003), while grains are expected to grow and survive at even larger distances.

In this sense, another mechanism must be used to accelerate the gas near surface. The most promising mechanism for the winds of cool stars is the transfer of momentum and energy to the wind from MHD waves. Alfvén waves driven wind models are known to result in high velocity winds, unlike what is measured for giant cool stars, because these MHD waves are, in general, weakly damped. Hartmann & MacGregor (1980) showed that it would be possible to re-

* E-mail: diego@astro.iag.usp.br

produce the observed low wind velocities and the high mass loss rates of the cool giant and supergiant stars if some kind of wave damping mechanism is effective at the wind basis ($r < 2 R_*$). In that work, they confirmed this assumption using the ion-friction damping, which has a damping length proportional to P^2 , where P is the wave period. Holzer, Fla & Leer (1983) questioned this result in terms of an unnatural fine-tuning for the wave flux period, and argued that stars would, more reasonably, present a wide variety of wave frequencies depending on the generation mechanisms, and for most of them the damping would be ineffective. However, Jatenco-Pereira & Opher (1989) studied the effects of both different damping mechanisms and the magnetic field divergence, showing that the fine-tuning of the wave period is unnecessary since there are several other damping mechanisms that would act on the frequency spectrum. Also, they showed that the magnetic field divergent geometry can rapidly dilute the wave flux and also slow down the wind. Their magnetic field geometry was based on empirical relations found from observations of the solar wind. This because in general, in lack of direct measurements of the magnetic field fluctuations and structure in other stars, we have to simply extrapolate our knowledge from solar observations.

Parker (1958) proposed that the solar wind is accelerated by the strong thermal pressure gradient in the transition region, where the gas temperature increases from $\sim 10^4$ K up to 10^6 K. However, it became clear in the following years that neither the solar radiation, nor acoustic waves generated in the photosphere, could account for the heating of the coronal base. The origin of the energy responsible for the heating and acceleration of the plasma is believed to be from both magnetic field reconnections above the photosphere (Axford & McKenzie 1996) and convective motions under the stellar surface. The convective energy is transferred up to the atmosphere from the perturbations generated in the field line footpoints (Cranmer & van Ballegooijen 2005). These perturbations propagate outwards as Alfvén waves, heating the gas as they are damped (Suzuki & Inutsuka 2005). Regarding the magnetic field lines, Holzer & Leer (1980) and Jatenco-Pereira & Opher (1989) realized that the super-radial geometry of the magnetic field funnels at the coronal holes could have a significant impact on the mass flux and wind speed. Esser *et al.* (2005), showed that the models considering highly diverging magnetic funnels explain better the observed data for the Sun. Also, Tu *et al.* (2005) established that the solar wind acceleration initiates in the magnetic funnels at heights lower than 2.10^9 cm, coincident with the high divergence region.

In this work, we model the acceleration and heating of a late-type supergiant stellar wind considering an outward flux of Alfvén waves. We solve the MHD equations to, self-consistently, determine the magnetic field geometry and the wind temperature, density and velocity profiles. In section 2, we describe the model basic equations. In section 3 we present the results and the discussions, followed, by the work conclusions.

2 THE MODEL

The wind equations are based on mass, momentum, energy and magnetic flux conservation. The first is given by:

$$\rho u A(r) = \rho_0 u_0 A(r_0), \quad (1)$$

where u is the flow velocity, ρ is the gas density and $A(r)$ is the flow cross-section area at a distance r from the center of the star. The index “0” indicates the variable is being evaluated at the stellar surface ($r = r_0$).

Assuming a steady flow, the momentum equation can be written as:

$$\rho(\vec{u} \cdot \vec{\nabla})\vec{u} = -\rho \frac{GM_*}{r^3} \vec{r} - \vec{\nabla}P - \vec{\nabla} \left(\frac{\langle (\delta B)^2 \rangle}{8\pi} \right) + \frac{1}{4\pi} (\vec{B} \cdot \vec{\nabla}) \vec{B} - \vec{\nabla} \left(\frac{B^2}{8\pi} \right), \quad (2)$$

where $P = \rho k_B T/m$ is the thermal pressure, k_B is the Boltzmann constant, T is the gas temperature, m is the mean mass per particle, G the gravitational constant and δB the wave magnetic field amplitude. In Equation (2), the right hand side contains the gravitational force density and the thermal and wave pressure gradients, respectively. The last two terms represent the Lorentz force. The wave amplitude (δB) is related to the wave energy density (ϵ) by $\epsilon = \langle (\delta B)^2 \rangle / (4\pi)$.

2.1 Thin fluxtube approximation

Typically, considering magnetic field strengths > 1 G, the wind basis is characterized by the relation $B^2/8\pi \gg P > \rho u^2/2$, *i.e.* the plasma is magnetically dominated. In this case, if we assume the wind to be initiated at funnels anchored at the stellar surface, which are surrounded by a plasma with lower magnetic field strength, the magnetic pressure inside will push the gas and the funnel field lines will expand. The funnel cross-section radius (\mathcal{R}) will grow super-radially up to a limit value (\mathcal{R}_m). This limiting cross-section radius depends both on the relation between external and internal magnetic field strengths and on the filling factor (α). As the area increases, the internal magnetic strength diminishes until the equilibrium between internal and external magnetic pressures is reached. If the internal magnetic field strength is much larger than the external, the flux tubes cross-section will depend on the filling factor only. The filling factor is the ratio between the area of the stellar surface covered by funnels and the total area. The averaged maximum area that a funnel could reach would be $A_m = A(r_0)/\alpha$ or, in terms of the cross section radius:

$$\mathcal{R}_m = \frac{\mathcal{R}_0}{\alpha^{1/2}}. \quad (3)$$

For the quiet Sun, the funnels that merge to form the coronal holes cover about 10% of the total surface.

To evaluate the tube expansion at the wind basis, we assume the plasma to be magnetically dominated and the left hand side of Equation (2) may be neglected if compared to the other terms. Then, by using $\vec{\nabla} \cdot \vec{B} = 0$ and a power series expansion method proposed by Pneuman, Solanki & Stenflo (1986), we can determine self-consistently the magnetic field geometry without assuming any empirical function for the funnel cross-section with distance.

Following Pneuman, Solanki & Stenflo (1986), using the thin fluxtube approximation, Equation (2) and $\vec{\nabla} \cdot \vec{B} = 0$ are described near stellar surface by:

$$4\pi \frac{\partial P}{\partial y} \simeq B_r \left(\frac{\partial B_y}{\partial r} - \frac{\partial B_r}{\partial y} \right), \quad (4)$$

$$4\pi \left(\frac{\partial P}{\partial r} + \frac{P}{H} \right) \simeq -B_y \left(\frac{\partial B_y}{\partial r} - \frac{\partial B_r}{\partial y} \right), \quad (5)$$

and

$$\frac{1}{y} \frac{\partial}{\partial y} (y B_y) + \frac{\partial B_r}{\partial r} = 0, \quad (6)$$

where $H = k_B T r^2 / G m M_*$ is the scale height.

Expanding all variables as power series in y (*i.e.* along the tube radius), and neglecting terms of orders higher than 2, Equations (4) – (6) give rise to a differential equation for the fluxtube cross section:

$$\frac{A(r_0)}{2H_0^2} \left[\frac{\partial^2}{\partial r^2} \left(\frac{A(r_0)}{A(r)} \right) - \frac{1}{2A(r)} \frac{\partial}{\partial r} \left(\frac{A(r_0)}{A(r)} \right) \right] = \left(\frac{A(r_0)}{A(r)} \right)^2 \left[1 - \left(\frac{B_{ext}}{B_0} \frac{(1-\alpha)}{\left(\frac{A(r_0)}{A(r)} - \alpha \right)} \right)^2 \right] + 2\beta \frac{P(r)}{P(r_0)}, \quad (7)$$

where $\beta = 4\pi P(r_0)/B^2(r_0)$, α is the filling factor and B_{ext} is the magnetic field strength outside the fluxtube. In the following calculations we fixed its value to be $10^{-3} B(r)$.

To simplify the set of equations, we will define the funnel area expansion as a function of radial distance by:

$$A(r) = A(r_0) \left(\frac{r}{r_0} \right)^S, \quad (8)$$

where S is the expansion index, which is super-radial ($S > 2$) at the wind basis up to the merging radius when S becomes 2. S is determined from Equation (7).

2.2 The energy equation

Falceta-Gonçalves & Jatenco-Pereira (2002) showed that, even though presenting low effective temperatures, the temperature gradients at the wind basis of late-type supergiant stars could play an important role in accelerating the gas, as occurs in the Sun. In their model, the temperature profile was assumed to be a r dependent function, obtained from observational data. The wind temperatures in giant cool stars are expected to increase from the photospheric value up to 10^4 K, much lower than what is observed for the Sun, but still important in the wind acceleration if the gradient occurs in small lengthscales. From their calculations, Falceta-Gonçalves & Jatenco-Pereira (2002) also showed that the thermal pressure is even more important than radiation pressure at the non-pulsating phase of these objects.

In a consistent model, to avoid assuming any empirical function for the magnetic field geometry and to determine the wind temperature at each wind position (r), we have to solve the energy equation, which is determined from the balance between wave heating and the adiabatic expansion and radiative coolings (Hartmann, Edwards & Avrett 1982; Vidotto & Jatenco-Pereira 2006). Thus, neglecting conduction, we write the energy equation as:

$$\rho u \frac{d}{dr} \left(\frac{u^2}{2} + \frac{5 k_B T}{2 m} - \frac{G M_*}{r} \right) + \frac{u}{2} \frac{d\epsilon}{dr} = (Q - P_R), \quad (9)$$

where $\epsilon = \langle (\delta B)^2 \rangle / (4\pi)$ is the wave energy density, which

is described below (Sec. 2.3), Q is the wave heating rate, *i.e.* the rate at which the gas is being heated due to dissipation of wave energy, and P_R is the radiative cooling rate, both in $\text{erg cm}^{-3} \text{ s}^{-1}$. The wave heating can be written as:

$$Q = \frac{\epsilon}{L} (u + v_A) \quad (10)$$

and the radiative cooling is given by:

$$P_R = \Lambda n_e n_H, \quad (11)$$

where n_e is the electron density, n_H is the hydrogen density and Λ is the radiative loss function. Here, we adopt the Λ function given by Schmutzler & Tscharnuter (1993) and calculate n_e with the modified Saha equation given by Hartmann & MacGregor (1980).

2.3 Wave energy density

The wave energy density at each step may be calculated, using a WKB approximation, from the wave action conservation. Under this assumption, the wave energy density is dissipated as follows:

$$\epsilon = \epsilon_0 \frac{M_0}{M} \left(\frac{1 + M_0}{1 + M} \right)^2 \exp \left[- \int_{r_0}^r \frac{1}{L} dr' \right], \quad (12)$$

where $M = u/v_A$ is the Alfvén-Mach number, $v_A = (B/\sqrt{4\pi\rho})$ the Alfvén speed and L the wave damping length. Also, the wave flux (ϕ_A) at r_0 is evaluated by (Jatenco-Pereira & Opher 1989):

$$\phi_{A_0} = \epsilon_0 v_{A0} \left(1 + \frac{3}{2} M_0 \right). \quad (13)$$

Actually, the WKB approximation is not valid when the perturbation wavelength is much larger than the gradients lengthscales of the system, *e.g.* when $\lambda > L$. As a consequence, part of the wave flux is reflected and the Alfvén waves propagating on opposite directions decay as the generated beat waves interact with the gas particles. Davila (1985) pointed out that, in the Sun, the gradients of the coronal parameters are high enough to make the WKB approximation not applicable. However, Usmanov *et al.* (2000) found good agreement between the observational data and models with this approach. In this model, we used Equation (12) assuming then linear perturbations, however included non-linear effects in the damping length function (L_{NL}). The non-linear damping length is given by (Jatenco-Pereira & Opher 1989):

$$L_{NL} = L_0 \left(\frac{v_A}{v_{A0}} \right)^4 \frac{\langle (\delta v)^2 \rangle_0}{\langle (\delta v)^2 \rangle} (1 + M), \quad (14)$$

where $\langle (\delta v)^2 \rangle$ is the averaged squared perturbation velocity amplitude and L_0 is the damping length at the wind basis, which is mainly dependent on the assumed wave frequency spectrum (Lagage & Cesarsky 1983). Here, we will let it as a free parameter.

2.4 The wind equations

Finally, once the magnetic field structure is determined, we evaluate the temperature and velocity of the wind along the magnetic field. Using the Equation (8) and considering the magnetic flux conservation, Equations (1), (2) and (9) in the

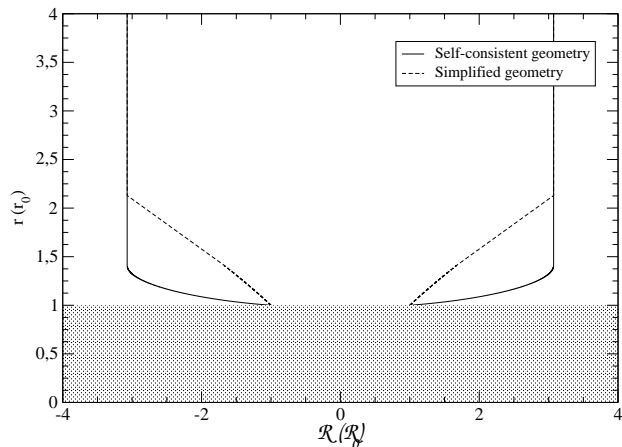


Figure 1. The magnetic field structure for a constant super-radial index $S = 5$ (dashed line) and that determined self-consistently in our model (solid line).

radial direction are reduced to (Vidotto & Jatenco-Pereira 2006):

$$\frac{dT}{dr} = \frac{2T}{3r} \left[\frac{r(Q - P_R)}{\rho u (k_B T / m)} - \left(S + \frac{r}{u} \frac{du}{dr} \right) \right], \quad (15)$$

and

$$\begin{aligned} \frac{1}{u} \frac{du}{dr} \left[u^2 - \frac{5 k_B T}{3 m} - \frac{\langle (\delta v)^2 \rangle}{4} \left(\frac{1 + 3M}{1 + M} \right) \right] = \\ = \frac{S}{r} \left[\frac{5 k_B T}{3 m} - \frac{2 r(Q - P_R)}{3 S \rho u} - \frac{GM_*}{rS} + \right. \\ \left. + \frac{\langle (\delta v)^2 \rangle}{2LS} r + \frac{\langle (\delta v)^2 \rangle}{4} \left(\frac{1 + 3M}{1 + M} \right) \right]. \quad (16) \end{aligned}$$

Equations (13) – (16) fully describe the wind parameters and the magnetic field geometry under the given assumptions. In the next section, we show the main results by applying these equations in a typical cool supergiant star and compare them with previous works.

3 RESULTS AND DISCUSSIONS

For the last decades, the validity of a wind model was constrained in reproducing only both the terminal velocity and the mass-loss rate of a given star. As a consequence, a number of accelerating mechanisms were found in accordance to observations of these constrains. However, with the high resolution observations and more sensitive instruments the parameters radial profiles will become measurable and will be decisive on the modelling choice. Here we determine the velocity, density and temperature profiles and discuss their dependence on initial assumptions.

We applied the described model on a cool supergiant star with $M_* = 16 M_\odot$, $r_0 = 400 R_\odot$, $\rho_0 = 10^{-13} \text{ g cm}^{-3}$, $B_0 = 10 \text{ G}$ and $T_0 = 3500 \text{ K}$. We also assumed a filling factor $\alpha = 0.1$, according to solar observations.

3.1 Wind profiles

To study the importance of the damping length on the wind profiles we performed calculations setting the initial wave

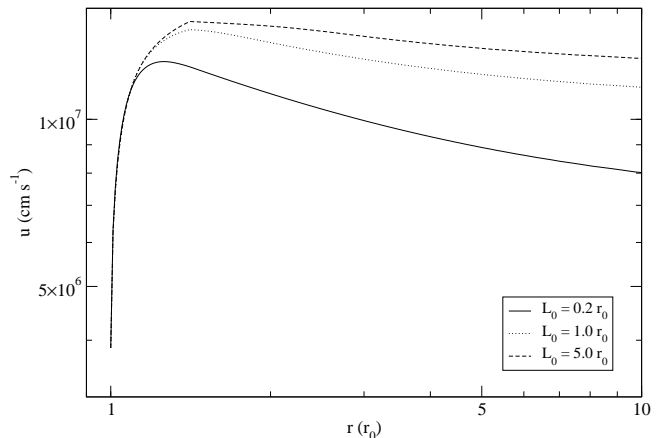


Figure 2. Wind velocity profiles obtained for the initial damping lengths $L = 0.2 r_0$ (solid line), $L = 1.0 r_0$ (dotted line) and $L = 5.0 r_0$ (dashed line) as function of the distance.

flux as $\phi_{A0} = 3.10^7 \text{ erg cm}^{-2} \text{ s}^{-1}$, and varied L_0 as 0.2, 1.0 and $5.0 r_0$. The magnetic field structure is shown in Figure (1). The solid line represents the solution of Equation (7) for the given stellar parameters, compared to a simple constant expansion factor $S = 5$ (dashed line), as used by Falceta-Gonçalves & Jatenco-Pereira (2002). Comparing both curves we find that the self-consistent geometry is more divergent near stellar surface, and the flux tubes are expected to merge at lower distances, in agreement with more refined models for the Sun (Esser *et al.* 2005). We obtained an initial value of $S(r_0) \simeq 35$, that decreases with distance to the stellar surface. From the assumed α , we found that the neighbour fluxtubes merge at $r = 1.41 r_0$. At this point, with a sudden decrease of S from its super-radial value to $S = 2$ (radial), the wind properties change and it is noticeable as breaks in the temperature, density and velocity profiles.

We obtained the same geometry for the following calculations considering different initial parameters. This because the super-radial magnetic field geometry occurs mainly at the wind basis, where the magnetic pressure is highly dominant. In this sense, we expect the expansion index (S) to be independent on the other initial parameters such as the wind velocity, the wave flux densities and the damping length.

In Figure (2) we compare the wind velocity profiles for the different initial damping lengths. As expected, the larger the damping length the higher is the wind velocity. However, for previous works that do not take into account any high initial divergence, the wind velocity is even larger. The obtained divergence result in a fast dilution of the wave energy density near the stellar surface. As a consequence, the lack of wave flux at larger distances results in lower velocities. This result shows that even low damped wave fluxes can be responsible for low terminal velocities, depending on the field divergence.

In Figures (3) – (5) we present the gas mass density, wave energy density and the temperature, respectively, for the same calculations. For the gas density, all three lines show the same behaviour at $r < 1.5 r_0$ indicating that the flux tube divergence is the dominant factor if comparing to the gas expansion due to acceleration. This is an interesting result since, typically, the density profile is believed to be closely related to the velocity profile only. In Figure (4),

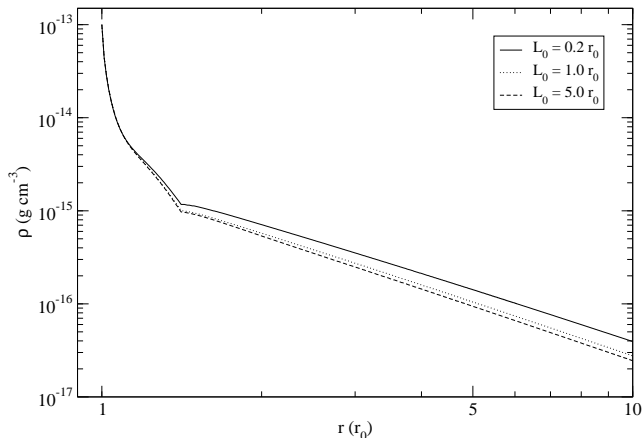


Figure 3. Wind density profiles obtained for the initial damping lengths $L = 0.2 r_0$ (solid line), $L = 1.0 r_0$ (dotted line) and $L = 5.0 r_0$ (dashed line) as function of the distance.

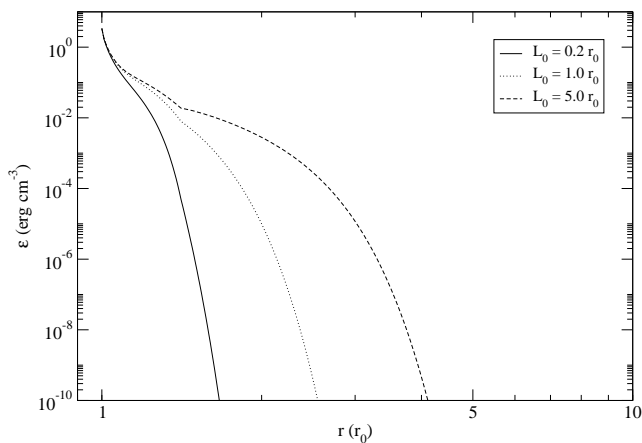


Figure 4. Wave energy density profiles obtained for the initial damping lengths $L = 0.2 r_0$ (solid line), $L = 1.0 r_0$ (dotted line) and $L = 5.0 r_0$ (dashed line) as function of the distance.

we notice that, in despite of what was obtained in previous works, the wave energy density is weakly dependent on the initial damping length at the wind basis. This mainly because, again, the field divergence is dominant on the dilution process. On the other hand, for distances larger than the flux tubes merging position the wave damping is dominant. In Figure (5), the temperature profiles show different features. For the given stellar parameters, if $L_0 = 5.0 r_0$, the wave heating is less effective and the radiative losses added to the expansion cooling result in a negative temperature gradient, which occurs in a very narrow region until the density becomes low enough for the radiative losses become less important. For highly damped waves, the wave heating dominates the radiative losses and the temperature gradient is positive near the surface. Another interesting feature is the maximum temperature position. Since the temperature gradient is mainly dependent on the wave damping (*via* Q parameter), we notice that the lower is the damping length, the closer to the stellar surface the maximum temperature occurs.

Recently, Zeeman splitting of H_2O masers observations led Vlemmings, Diamong & van Langevelde (2002) to in-

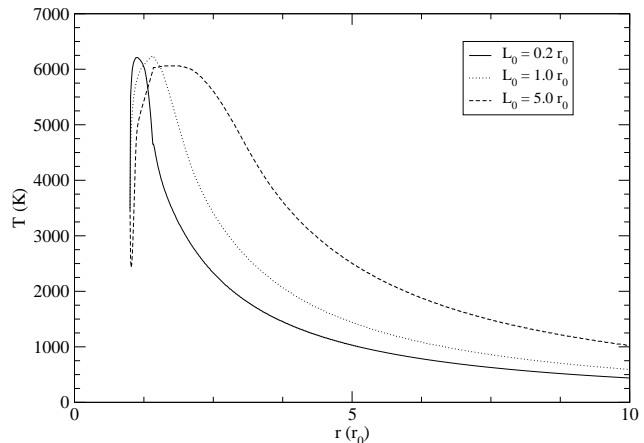


Figure 5. Wind temperature profiles obtained for the initial damping lengths $L = 0.2 r_0$ (solid line), $L = 1.0 r_0$ (dotted line) and $L = 5.0 r_0$ (dashed line) as function of the distance.

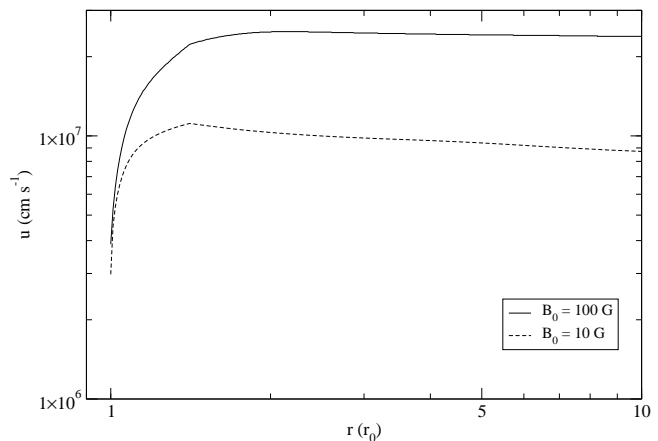


Figure 6. Wind velocity profiles obtained for initial magnetic field strengths $B_0 = 10$ G (dotted line) and $B_0 = 100$ G (solid line) as function of the distance.

fer magnetic field strengths on supergiant stellar surfaces of $B_0 > 100$ G. Also, theoretical dynamo models for AGB stars reveal that the planetary nebulae shapes can be explained by magnetic field strengths of ~ 200 G (Blackman *et. al.* 2001). For this reason, we also performed numerical calculations for $B_0 = 10$ and 100 G, setting the initial parameters for a low damped wave flux ($L_0 = 5 r_0$). We also assumed the same wave amplitude relative to the magnetic field for both cases.

The velocity profile for both initial magnetic field strengths are shown in Figure (6). For the larger magnetic field strength ($B_0 = 100$ G) we obtained the higher terminal velocity ($u > 200 \text{ km s}^{-1}$). This effect is mainly due to the higher wave energy flux assumed at the wind basis to accomplish the same relative wave amplitude.

The temperature profiles, shown in Figure (7), also present features dependent on the magnetic field strength. As for the velocity, a high wave energy flux results in a high temperature, at least near the stellar surface due to the higher energy density.

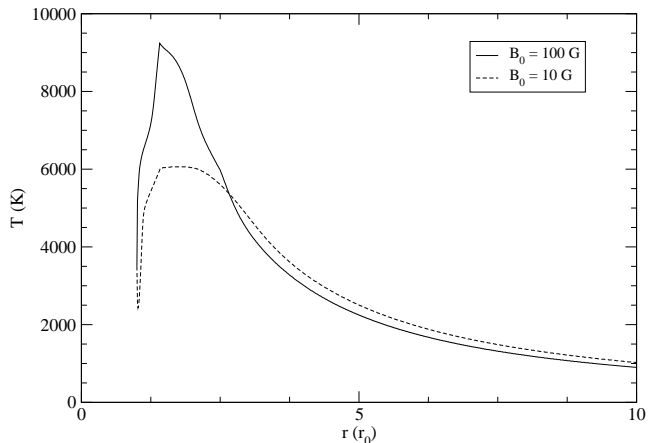


Figure 7. Wind temperature profiles obtained for initial magnetic field strengths $B_0 = 10$ G (dotted line) and $B_0 = 100$ G (solid line) as function of the distance.

3.2 Best-fitting model

For stars with parameters similar to those used in the previous subsection, observational data reveal typical mass-loss rates of $\dot{M} \simeq 10^{-7} - 10^{-6} M_\odot \text{ yr}^{-1}$ and terminal velocities of $u \simeq 70 \text{ km s}^{-1}$. Unfortunately, the available data are limited in spatial resolution for most of the stars, and it is not possible to fit the complete radial profiles.

Assuming a surface magnetic field strength $B_0 = 10$ G, and a low damped wave flux ($L_0 = 5 r_0$), it was possible to reproduce both the wind terminal velocity and the mass loss rate using an Alfvén waves flux of $\phi_{A0} = 10^7 \text{ erg cm}^{-2} \text{ s}^{-1}$ at the wind basis. This value corresponds to a wave amplitude of $(\langle \delta B \rangle^2)^{\frac{1}{2}} \simeq 3.10^{-2} B_0$, which is very plausible for a turbulent medium as that at the stellar surface.

The velocity and temperature profiles for this case are shown in Figures (8) and (9), respectively. The velocity profile reveals a peak of $u > 100 \text{ km s}^{-1}$ at $r < 2.0 r_0$, and slightly decreases for larger distances until reaching the observed value. The temperature profile presents an initial negative gradient reaching temperatures $T < 2500$ K in a narrow region. Also, near $r = 1.5 r_0$ the temperature reaches the maximum value of ~ 6000 K. For $r > 3.0 r_0$, where the wave heating and the radiative losses are low, the temperature decreases due to the adiabatic expansion.

4 CONCLUSIONS

We propose a self-consistent wind model to determine the parameters profiles for a supergiant late-type star. To determine the magnetic field geometry we used an expansion method over the wind physical parameters as proposed by Pneuman, Solanki & Stenflo (1986). Near surface, the magnetic pressure inside the flux tubes are higher than that of the surrounding medium, forcing the field lines to curve. We found an initial super-radial expansion factor $S > 30$ at the wind basis, much higher than the value used by previous authors that included empirical relations to account for the magnetic field geometry based on solar observations.

Considering a supergiant late-type star with $M_* = 16 M_\odot$, $r_0 = 400 R_\odot$, $\rho_0 = 10^{-13} \text{ g cm}^{-3}$, $B_0 = 10$ G and

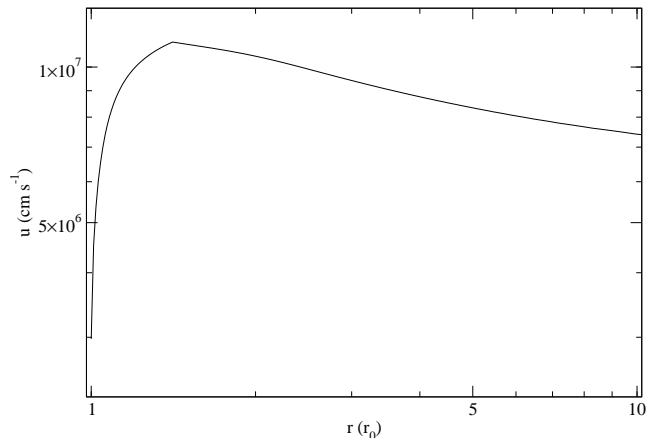


Figure 8. The wind velocity profile for the best fitting parameters in the case of low damped waves. Here we assumed $B_0 = 10$ G, $L_0 = 5.0 r_0$ and $\phi_{A0} = 10^7 \text{ erg cm}^{-2} \text{ s}^{-1}$.

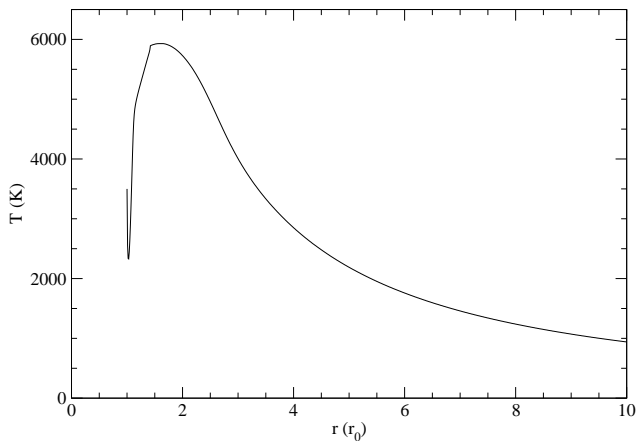


Figure 9. The wind temperature profile for the best fitting parameters in the case of low damped waves. Here we assumed $B_0 = 10$ G, $L_0 = 5.0 r_0$ and $\phi_{A0} = 10^7 \text{ erg cm}^{-2} \text{ s}^{-1}$.

$T_0 = 3500$ K, we obtained the wind velocity, density and temperature profiles. Typically, Alfvén wave driven winds result in high velocity winds ($u > 100 \text{ km s}^{-1}$), unless some strong wave damping mechanism takes place at the wind basis. We showed that this conclusion is correct in the case of low divergent magnetic field structures. In this work, the strong divergence is responsible for a rapid wave spatial dilution near surface, resulting in a lower wind velocity even for low damped waves.

We reproduced both the typical mass-loss rate ($\dot{M} \simeq 10^{-7} - 10^{-6} M_\odot \text{ yr}^{-1}$) and terminal velocity ($u \simeq 70 \text{ km s}^{-1}$) observed for these objects, assuming a weakly damped ($L_0 = 5.0 r_0$) Alfvén wave flux of $\phi_{A0} = 10^7 \text{ erg cm}^{-2} \text{ s}^{-1}$. The velocity profile reveals an efficient acceleration at $r < 1.5 r_0$, reaching the maximum value $\sim 100 \text{ km s}^{-1}$. In this region the wind is mainly accelerated by the wave energy density and the thermal pressure gradients. Afterwards, the absence of the wave acceleration and the cooling gas result in a decrease of the velocity to the observed values. For the temperature, assuming a weakly damped wave flux, the radiative losses and the expansion cooling are dominant near surface, and the temperature gradient is initially negative.

The temperature falls to $\simeq 2500$ K in a sharp region and then, as density decreases as the wind accelerates and the flux tube expands, it increases up to $\simeq 6000$ K at $r < 2.0 r_0$. For higher distances, where the radiative losses are low and the wave heating is no longer effective, the temperature decreases mainly due to the adiabatic expansion.

ACKNOWLEDGMENTS

D. Falceta-Gonçalves and A. A. Vidotto thank the Brazilian agency FAPESP for the financial support (04/12053-2 and 04/13846-6). V. Jatenco-Pereira thanks CNPq for the financial support (304523/90-9).

REFERENCES

- Airapetian, V. S., Carpenter, K. & Ofman, L. 2003, AAS, 202, 3214
- Axford, W. I. & McKenzie, J. F. 1996, Ap&SS, 243, 1
- Blackman, E. G., Frank, A., Markiel, J. A. *et al.* 2001, Nature, 409, 485
- Cranmer, S. R. & van Ballegoijen, A. A. 2005, ApJS, 156, 265
- Davila, J. M. 1985, ApJ, 291, 328
- Dupree, A. K. 1986, ARA&A, 24, 377
- Elitzur, M. & Ivezić, Z. 2001, MNRAS, 327, 403
- Esser, R., Lie-Svendsen, O., Janse, A. M. *et al.* 2005, ApJ, 629, 61
- Falceta-Gonçalves, D. & Jatenco-Pereira, V. 2002, ApJ, 576, 976
- Guandalini, R., Busso, M., Ciprini, S. *et al.* 2005, astro-ph 0509739
- Hartmann, L. & MacGregor, K. B. 1980, ApJ, 242, 260
- Hartmann, L., Edwards, S., & Avrett, E. 1982, ApJ, 261, 279
- Holzer, T. E., Fla, T. & Leer, E. 1983 ApJ, 275, 808
- Holzer, T. E. & Leer, E. 1980, JGR, 85, 4665
- Jatenco-Pereira, V. & Opher, R. 1989, A&A, 209, 327
- Lamers, H. J. G. L. M. & Cassinelli, J. P. 1999, Introduction to Stellar Winds (New York: Cambridge Univ. Press)
- Lagage, P. O. & Cesarsky, C. J. 1983, A&A, 125, 249
- Liberatore, S., Lafon, J. & Berruyer, N. 2001, A&A, 377, 522
- Parker, E. N. 1958, ApJ, 128, 664
- Pneuman, G. W., Solanki, S. K. & Stenflo, J. O. 1986, A&A, 154, 231
- Sandin, C. & Hofner, S. 2003, A&A, 404, 789
- Schmutzler, T., & Tscharnuter, W. M. 1993, A&A, 273, 318
- Suzuki, T. K. & Inutsuka, S. 2005, at Solar Wind 11/SOHO 16 Conf., Canada (astro-ph 0508568)
- Tu, C., Zhou, C., Marsch, E. *et al.* 2005, Science, 308, 519
- Usmanov, A. V., Goldstein, M. L., Besser, B. P. & Fritzer, J. M. 2000, JGR, 105, 12675
- Vidotto, A. A. & Jatenco-Pereira, V. 2006, ApJ, 639, 416.
- Vlemmings, W. H. T., Diamond, P. J. & van Lengevelde, H. J. 2002, A&A, 394, 589
- Woitke, P. & Niccolini, G. 2005, A&A, 433, 1101